Journal of Directed Energy, **4**, Winter 2010, 205–222

Optimum Beam Wavelength for Laser-Based Directed Energy Systems and Electrostatic Mitigation Approach for Uninterrupted Telemetry during Testing

Madhusudhan Kundrapu* **and Michael Keidar†**

Department of Mechanical and Aerospace Engineering, The George Washington University, Washington, D.C. 20052

and

Charles Jones‡

Air Force Flight Test Center, 812TSS/ENIE, Edwards Air Force Base, CA 93524

Laser beams of directed energy systems lose a significant amount of energy before they reach the target surface, due to atmospheric attenuation, plasma shielding, and target surface reflection. The energy losses depend on the beam wavelength. A detailed numerical analysis is carried out to optimize the beam wavelength, in order to achieve identical rates of destruction with low fluences, for three different target surfaces made of Al, Cu, and Ti. Plasma formed due to laser target interaction attenuates telemetry during testing of directed energy systems. An electrostatic approach for the mitigation of communication attenuation is analyzed to obtain the fluency limits up to which the approach can be implemented. The effect of background pressure on the bias voltage requirement to create a sheath is analyzed. A self-consistent numerical model that couples laser–target interaction with plasma formation and plume expansion is employed to obtain the evaporation rates and plasma parameters. Transient sheath calculations are performed to characterize the sheath. Ablation analysis shows that the optimum wavelength for Al is 850 nm. It is found from sheath calculations that uninterrupted telemetry can be achieved through Al plasma for fluences below 4 J/cm^2 at a background pressure of 1 atm, using a maximum bias voltage of 10 kV.

KEYWORDS: Directed energy, Electrostatic sheath, Laser ablation, Optimum wavelength

Received July 13, 2009; revision received September 15, 2010

*Corresponding author; e-mail: madhusnk@gmail.com.

†E-mail: keidar@gwu.edu.

‡E-mail: charles.jones@edwards.af.mil.

Nomenclature

c	speed of light
e	charge of electron
h	Planck constant
I	irradiance of laser beam before reaching plasma
I_0	irradiance of laser beam at target surface
k	imaginary part of index of refraction
k_b	Boltzmann constant
m_e	mass of electron
n	real part of index of refraction
n_e	number density of electrons
$n_{e\,\max}$	peak density of electrons
n_{iZ}	number density of ions of ionized state Z
n_0	number density of neutrals
p	pressure
Q	photon absorption cross section
Q_{laser}	laser energy
R	coefficient of reflectivity
s	thickness of sheath
s_0	thickness of sheath using Child–Langmuir relation
T	temperature
U	voltage across sheath
V	velocity
Z_i	average charge number of ions
z	coordinate axis
$z_{ne\,\max}$	location of peak density of electrons
α	absorption coefficient of the solid material
$\alpha_{e\text{-}i}$	inverse Bremsstrahlung electron-ion absorption coefficient of plasma
$\alpha_{e\text{-}n}$	inverse Bremsstrahlung electron-neutral absorption coefficient of plasma
ε_0	permittivity of vacuum
ε_{rad}	reradiation of plasma
λ	laser beam wavelength
ν	frequency of laser beam

1. Introduction

Directed energy weapon (DEW) systems use concentrated electromagnetic radiation in order to disable or destroy a stationary or moving target. The DEW and/or target may be located on the ground, in the air, or in space. Development and testing of DEWs involve the evaluation of the effect of weapons on the target and the assessment of defensive capabilities of the target.[2] If the energy beam wavelength is in the range of a few nanometers to a micrometer, then the weapons are categorized under laser-based DEW. The laser beam diameter can be as large as 50 cm, with power ranging from several kilowatts to gigawatts per square centimeter. The power characteristics of the beam, such as fluence and duration, depend on the type of target and objectives of the mission. The target and/or weapon can be stationary, low speed, or high speed and located on ground, in the air, or in space. The mission objectives may be to (1) temporarily disable or permanently damage the target's

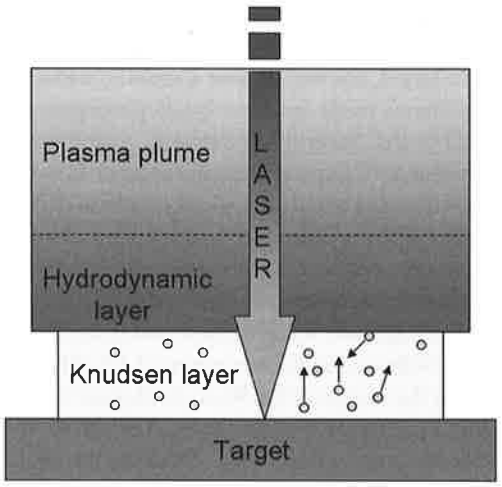

Fig. 1. Schematic of laser ablation.

optronic sensors and radio communication devices or (2) destroy the target completely. If the weapon–target engagement duration is long enough, as in the case of stationary targets, low-energy lasers can be used to heat the target continuously. For instance, a laser pulse of 1 ms with 5 kJ of energy was used to destroy an optronic device located at a distance of 2 km and blind the same located 7 km away.[24] For targets such as missiles, which have a shorter duration of engagement, short pulses with high energy fluence are employed to fulfill the mission objectives.

For medium- and high-energy laser weapons with fluence >1 J/cm^2, the method of destruction is through laser ablation. The basic phenomena of laser ablation are shown in Fig. 1. When a high-energy laser beam is directed onto the target, it melts and evaporates the target to create a vapor cloud surrounding the ablation spot. The vapor and target are separated by a thin discontinuity layer known as the Knudsen layer (KL). Quite often the vapor temperature reaches above its ionization potential and transforms into plasma. A small region in the plume, which consists of weakly ionized plasma, near the target surface is known as the hydrodynamic layer (HL).[9] The remaining portion of the plume consists of strongly ionized plasma.

When a laser beam is directed from the weapon onto a distant target, a large amount of beam energy is lost due to several effects, such as (1) atmospheric attenuation (absorption, turbulence, scattering, and thermal blooming),[22] (2) plasma shielding near the target, and (3) surface reflectivity of the target.[20] The atmospheric attenuation follows Beer's law, and the attenuation coefficient depends on the laser beam wavelength (λ).[23] Absorption of irradiance in plasma near the target surface, known as plasma shielding, is mainly due to inverse Bremsstrahlung electron-neural and electron-ion processes.[1,25] Because inverse Bremsstrahlung coefficients $\alpha_{e\text{-}n}$ and $\alpha_{e\text{-}i}$ are functions of wavelength, the absorption of energy by plasma depends on wavelength. Besides this, the target surface reflectivity increases with wavelength,[18] which decreases the amount of energy absorbed by a target. Laser ablation of a Cu target showed that shorter wavelength results in a better ablation rate.[5] It is also observed that plume length increases with wavelength.[3] Because all the processes in laser ablation are strongly coupled, a detailed numerical analysis is required to investigate the dependency of ablation rate on wavelength.

By obtaining the wavelength for which ablation rates are maximum, the kill performance of the DEW can be achieved with lesser amounts of beam energy. On the other hand, if the objective is to defend a target, one can choose a suitable surface coating that minimizes the ablation rate. Measurements made for laser beam propagation in air at sea level over a distance of 1,800 m show that several atmospheric windows (wavelengths for which attenuation is low) are available in the wavelength range of 0.3–15 μm. (Refs. 8 and 23). However, the ablation rates are expected to be high at shorter wavelengths due to low surface reflectivity. So, in this paper we have considered wavelength in the range of 193–1,064 nm to carry out a detailed numerical analysis for finding the dependency of ablation rate on wavelength. Because the material response, in terms of evaporation and surface properties, varies differently with wavelength and fluence, three different materials, Al, Cu, and Ti, are considered for the analysis with a wide fluence range of 10–100 J/cm^2.

One of the major tasks in the design of DEWs is to choose the beam parameters such as energy fluence to destroy a particular type of target. The duration of engagement is very short for direct observations; hence continuous telemetry has to be established from the test bed to track the parameters such as temperature history. But the telemetry is often interrupted by the plasma shroud around the target. If the plasma frequency exceeds the radio wave frequency, then significant attenuation occurs. Though there is a possibility of isolating an antenna from plasma (by locating it away from ablation spot), this is not guaranteed for all encounters, in particular for spinning and small flying targets such as missiles. Besides this, if the goal is to defend the target's communication devices, then one has to consider the options to mitigate the attenuation of radio waves.

Several approaches have been suggested to mitigate this communication attenuation.[12-14,19] The most suitable approaches among those are electromagnetic and electrostatic. The electromagnetic approach employs an E $\times$ B layer in the plasma to accelerate plasma in a direction normal to and away from it. The density of plasma decreases above the layer, and hence plasma frequency also decreases. By choosing suitable values for the electric and magnetic fields, the plasma frequency can be reduced below that of radio wave frequencies. The electrostatic approach involves the introduction of a negatively biased electrode to create an electron-depleted sheath within the plasma. The advantage of the latter approach is design simplicity, and it eliminates almost all the electrons within the sheath. On the other hand, this study can also be used to specify the laser fluence to create a plasma shroud, around the antenna of the target, with electron density sufficient enough to interrupt communication.

In this paper we have evaluated the feasibility of the electrostatic approach for laser-ablated plasmas and carried out a detailed theoretical analysis for Al and Ti plasmas to find the fluence limits up to which this approach is applicable. Because the plasma frequency depends on electron density, which changes with background pressure, calculations were performed to find the influence of background pressure on bias voltage to create a sheath of required size to allow uninterrupted telemetry. Experimental validation of the analysis goes well beyond the scope of this paper.

2. Numerical Model

2.1. Self-consistent model for ablation

The computational domain is shown in Fig. 2. One-dimensional transient heat conduction in the enthalpy form is used for the target. Energy input to the target is calculated using

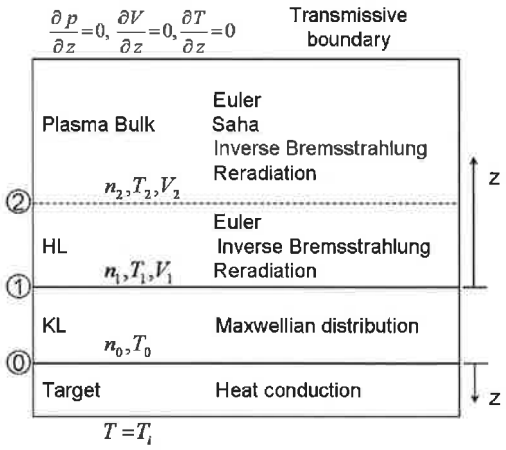

Fig. 2. Computational domain for laser ablation process.

Eq. (1), where $I_0(t)$ is the laser irradiance at the target surface. The absorption coefficient α and normal incidence of reflectivity R are functions of λ and evaluated using Eqs. (2) and (3). n and k are the real and imaginary parts of the effective index of refraction of a material. The Maxwellian distribution of velocity shifted by V_1 is considered in KL.[4,11] Euler equations are employed for the plasma plume while accounting for energy exchange with the laser beam. The ionization fraction of species in vapor is obtained using the Saha equation, and energy absorption by plasma is obtained by evaluating inverse Bremsstrahlung coefficients [Eqs. (4) and (5)] as functions of time and space. The irradiance at the target $I_0(t)$ is obtained from the actual irradiance of laser beam $I(t)$ by using these absorption coefficients and assuming the reflectivity of plasma to be zero in Eq. (1). Reradiation of energy from plasma is calculated using Bremsstrahlung radiation given by Eq. (6).

$$Q_{\text{laser}}(z,t) = \alpha(1-R)I_0(t)\exp\left(-\int_0^z \alpha\, dz\right), \tag{1}$$

$$\alpha = \frac{4\pi k}{\lambda}, \tag{2}$$

$$R = \frac{(n-1)^2 + k^2}{(n+1)^2 + k^2}, \tag{3}$$

$$\alpha_{e\text{-}n} = \left[1 - \exp\left(-\frac{\nu}{k_b T}\right)\right] Q n_e n_0, \tag{4}$$

$$\alpha_{e\text{-}i} = \left[1 - \exp\left(-\frac{\nu}{k_b T}\right)\right] \frac{4e^6 \lambda^3 n_e}{3hc^4 4m_e} \left(\frac{2\pi}{3m_e k_b T}\right)^{0.5} \sum_Z Z^2 n_{iZ}, \tag{5}$$

$$\varepsilon_{\text{rad}} = \left(\frac{2\pi k_b T}{3m_e}\right)^{0.5} \frac{32\pi e^6}{3hm_e c^3} n_e \sum_Z Z^2 n_Z. \tag{6}$$

The target thickness considered is sufficient to keep the nonablating end at initial temperature T_i. A transmissive boundary is assumed at the outer edge of the plume domain.

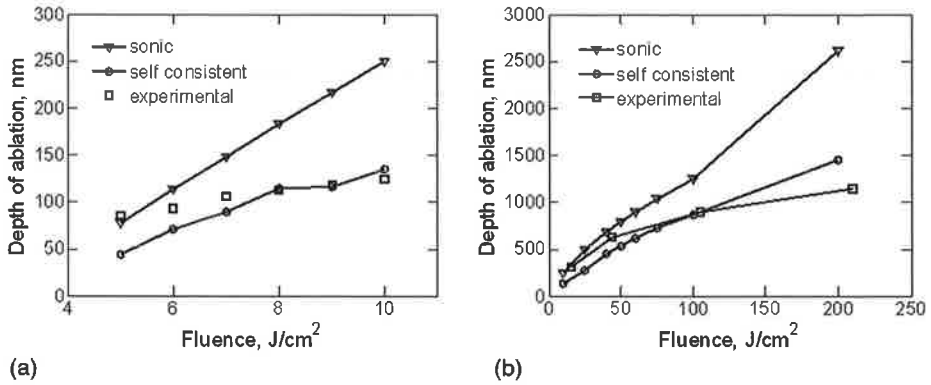

Fig. 3. Comparison of sonic and self-consistent models and validation with experimental results: (a) aluminum alloy 308 nm, 15 ns; experimental data are taken from Ref. 7; and (b) copper 532 nm, 6 ns; experimental data are taken from Ref. 21.

A nonuniform grid is used for both target and plasma domains. The first cell sizes in solid and fluid domains are 1 and 10 nm, respectively.

In most of the studies found in the literature, it was assumed that the thermodynamic state of vapor at the outer edge of the KL (interface-1) is that corresponding to Mach 1. The flow Mach number at interface-1 is actually dictated by the flow state outside the KL and is sonic only when the vapor pressure is large compared to the ambient pressure.[15] Because the pressure in the plume at the outer edge of the KL is comparable to the vapor pressure, in particular for high laser fluences, the sonic speed assumption may not give satisfactory results. So, a self-consistent model based on the ionization length scale in the hydrodynamic layer (HL) is employed to obtain a thermodynamic state at interface-1 as part of the iterative solution.[17]

The self-consistent model is compared with the sonic speed model and validated with experimental results of laser ablation of Al alloy[7] and Cu.[21] For Al alloy, a laser wavelength of 248 nm and 15-ns pulse duration with a 1–10 J cm^{-2} fluence range is considered, whereas for Cu, the wavelength is 532 nm and 6-ns laser pulse with a fluence range of 10–200 J cm^{-2}. Figure 3 demonstrates clearly that the self-consistent model shows good agreement with experimental results compared with the sonic speed model. Further details of the model can be found in Ref. 17.

2.2. Electrostatic sheath

The properties of plasma generated by laser ablation vary with time, and hence it is essential to consider transient sheath equations to obtain instantaneous sheath thickness in the plasma. Transient sheath thickness is calculated using Eq. (7). It is obtained by equating the Child law[6] ion current density with that at the plasma–sheath interface due to drift velocity V and the unsheathing of ions.[10] The electron density in Eq. (7) varies with time and space. By assuming electron density to be dependent only on time and its value equal to the peak density in the plume at any instant of time, Eq. (7) may be transformed into an ordinary differential equation. This can be solved analytically to obtain a simple expression for a transient sheath that is given by Eq. (8). The variable s_0 is given by Eq. (9), and V is velocity due to the Bohm criterion given by Eq. (10). Equation (8) is solved numerically

using the Newton–Raphson method in conjunction with the ablation model.

$$\frac{ds}{dt} = \frac{4}{9}\varepsilon_0 \left(\frac{2Z_i e}{m_i}\right)^{1/2} \frac{U^{3/2}}{s^2} \times \frac{1}{Z_i e n(z)} - V, \tag{7}$$

$$s = s_0 \frac{\exp\left[2(s + Vt)/s_0\right] - 1}{\exp\left[2(s + Vt)/s_0\right] + 1}, \tag{8}$$

where

$$s_0 = \left(\frac{4}{9}\varepsilon_0\right)^{1/2} \left(\frac{2Z_i e}{m_i}\right)^{1/4} \frac{U^{3/4}}{(eZ_i n V)^{1/2}}, \tag{9}$$

$$V = \left(\frac{k_b T}{m_i}\right)^{1/2}. \tag{10}$$

It has to be noted here that s_0 is the thickness of the sheath corresponding to the Child–Langmuir law.

3. Results

3.1. Laser beam wavelength

Ablation analysis is carried out with λ varying from 193 to 1,064 nm and laser fluence 10–100 J/cm^2. Three materials, Al, Cu, and Ti, are considered for the analysis. The real and imaginary parts of the index of refraction of the three materials for the considered wavelength range are taken from Ref. 10. It is observed that the optical properties of solid and molten Al are similar,[16] so the same values shown in Ref. 10 are considered for the respective molten states. A Gaussian profile laser pulse of 30-ns duration with full width at half-maximum (FWHM) at 8 ns is considered. Figure 4 shows the ablation characteristics and surface properties[18] of Al, Cu, and Ti. The subplots in the top row show the depth of ablation contours, percentage of energy absorbed by plasma, and surface properties as functions of wavelength, respectively, for Al metal. The subplots in the middle and bottom rows show similar contours and surface properties for Cu and Ti metals.

As expected, the depth of ablation of Al increases with the increase of laser fluence. But it increases gradually with wavelength until 850 nm and then decreases sharply. The maximum depth of ablation is found at 850 nm for all fluences, seemingly contradicting the plot shown for plasma shielding for Al, because the depth of ablation is maximum at the beam parameters for which the percentage of energy absorbed by plasma is highest. Since the energy absorbed by plasma due to inverse Bremsstrahlung process [Eqs. (4) and (5)] is directly proportional to the density of plasma, which in turn increases with the rate of evaporation, both maxima appear at more or less the same fluence and wavelength. The surface properties plot of Al shows that R remains more or less the same up to $\lambda = 450$ nm, decreases sharply until $\lambda = 850$ nm, and then increases sharply. Because R is lowest at $\lambda = 850$ nm, the heat flux at the Al surface is highest at this wavelength, and hence depth of evaporation is maximum.

Though R is constant in the range 190–532 nm, there is a gradual change in depth of evaporation due to changes in plasma shielding and α. It is difficult to find the exact influence of inverse Bremsstrahlung absorption as it is a function of temperature and plasma density, which depends on the instantaneous rates of evaporation. The rate of evaporation

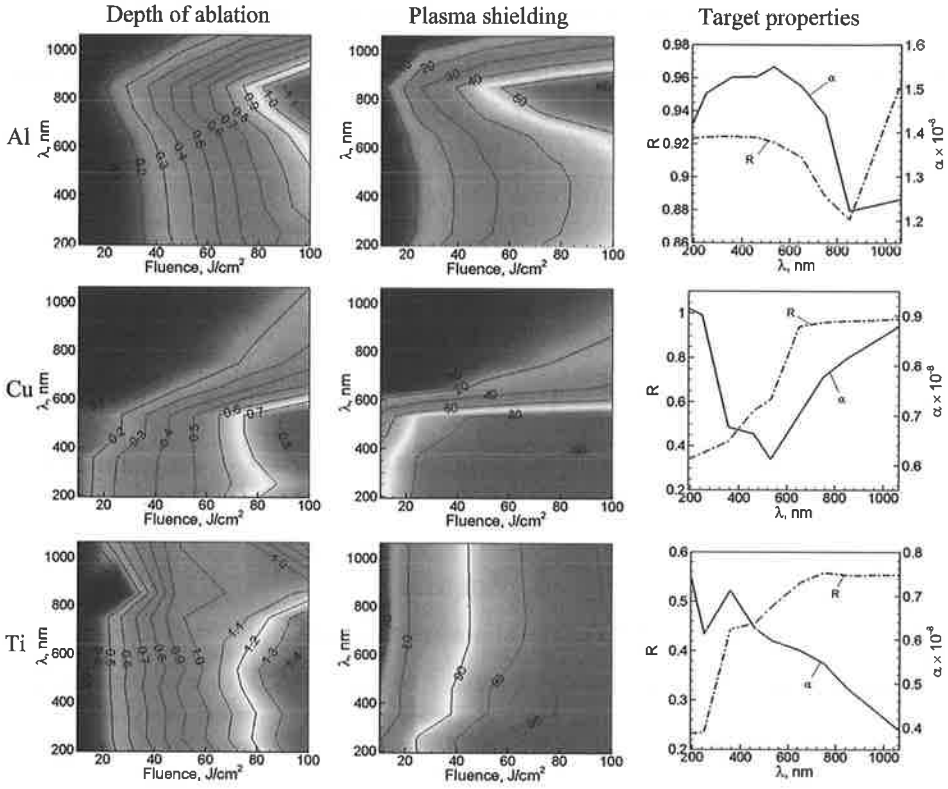

Fig. 4. Effect of laser beam wavelength and energy fluence on ablation of pure metals. Ablation characteristics of three metals, Al, Cu and Ti, are given in the top, middle, and bottom rows, respectively. The depth of ablation contours in micrometers is given in the first column, the percentage of energy absorbed by plasma is given in the second column, and surface properties are given in the third column. Surface properties are taken from Ref. 6.

in turn depends on the plasma parameters at the edge of the HL. So the effect of $\alpha_{e\text{-}n}$ and $\alpha_{i\text{-}n}$ is found indirectly by keeping $\alpha = 1.41 \times 10^8$ and $R = 0.921$ (values corresponding to $\lambda = 193$ nm) constant, while varying λ. For a fluence of 50 J/cm^2, the depth of ablation and percentage of energy absorbed are found to be 370 nm and 31.13% for $\lambda = 193$ and 402 nm and 29.94% for $\lambda = 532$ nm. This shows that the depth of ablation increases with the increase of λ. The actual depth of ablation for $\lambda = 532$ nm is 386 nm, which shows the effect of α, i.e., depth of ablation decreases when α is increased from 1.41×10^8 to 1.55×10^8. It is interesting to note here that the depth of ablation decreases with the increase in α; this is because the amount of energy absorbed with smaller α becomes greater than that absorbed with larger α after a certain depth. For instance, the amount of energy absorbed by Al with $\alpha = 1.41$ exceeds the energy absorbed with $\alpha = 1.55$ at a depth of 0.5 nm. However, the influence of $\alpha_{e\text{-}n}$, $\alpha_{i\text{-}n}$, and α on ablation depth is found to be very small when compared with the influence of R.

The trend of ablation contours of Cu shown in the middle row of Fig. 4 differs from that of Al. The depth of ablation is maximum at $\lambda \approx 360$ nm for fluences <50 J/cm^2, whereas

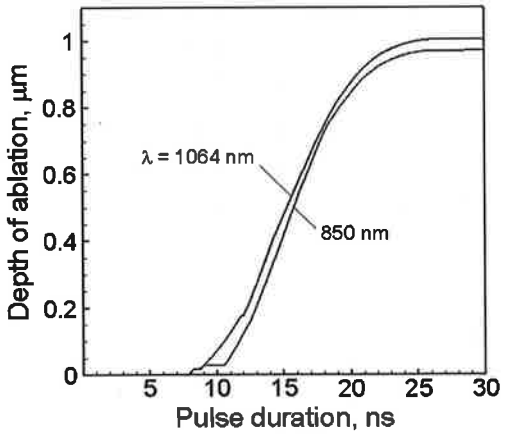

Fig. 5. Cumulative depth of evaporation of Ti target with a laser fluence of 50 J/cm^2.

it is maximum at $\lambda \approx 460$ nm for fluence >50 J/cm^2. This trend can be explained using the plasma shielding contours of Cu. For fluences <50 J/cm^2 and $\lambda < 360$ nm, plasma shielding is more or less constant so the ablation contours in this region display similar trends. For fluences >50 J/cm^2, the plasma shielding is highest for the lowest wavelength. At low λ, because the reflectivity is very low, ablation rates are high during the first half of the laser pulse. The high-density plasma formed will increase plasma shielding, and hence the ablation rate decreases. For instance, the ablation rate of Cu for $\lambda = 193$ nm and fluence of 100 J/cm^2 is greater than that for $\lambda = 460$ nm during the first 12 ns and it becomes less afterward. This shift in the time location increases with the decrease in fluence, and if it occurs in the second half of the pulse there will not be any noticeable change in the ablation characteristics. For higher wavelengths ($\lambda > 532$ nm), the depth of ablation decreases continuously as the reflectivity increases drastically.

Ablation contours of a Ti target are shown in the bottom row of Fig. 4. For fluences below 60 J/cm^2, the depth of ablation is slightly higher at $\lambda \approx 750$ nm, whereas for higher fluences above 60 J/cm^2, the maximum depth of ablation is observed for $\lambda \approx 532$ nm. For all the fluences, the depth of ablation decreases suddenly at $\lambda \approx 850$ nm, and then it increases with the increase in λ. At 850 nm, the sudden decrease in the depth of ablation is due to back flux. If the pressure at the evaporating surface is less than that of the surrounding plasma plume, then evaporation will not occur. Figure 5 shows the comparison of cumulative depth of evaporation for $\lambda = 850$ and 1,064 nm with fluence of 50 J/cm^2. It shows that back flux starts for both wavelengths at the same time, around 8 ns, but it extends to a greater duration for 850 nm compared to that of 1,064 nm. This is because of the difference in the energy absorbed by the surface. The reflectivity R is the same for both wavelengths, but α is small for 1,064 nm, which causes greater internal heat absorption that leads to higher surface temperature and evaporation pressure. Previously, it was observed in the case of Al ablation that the influence of α is less significant, but here in this case of Ti, it is influential to a considerable extent. This is because heat absorbed by the surface is directly proportional to R [Eq. (1)] and Ti has low reflectivity (0.75) compared to that of Al (0.92). It is interesting to observe from the subplot for plasma shielding of Ti that more than 90% of the laser energy is absorbed by plasma for fluences greater than 40 J/cm^2 for all wavelengths.

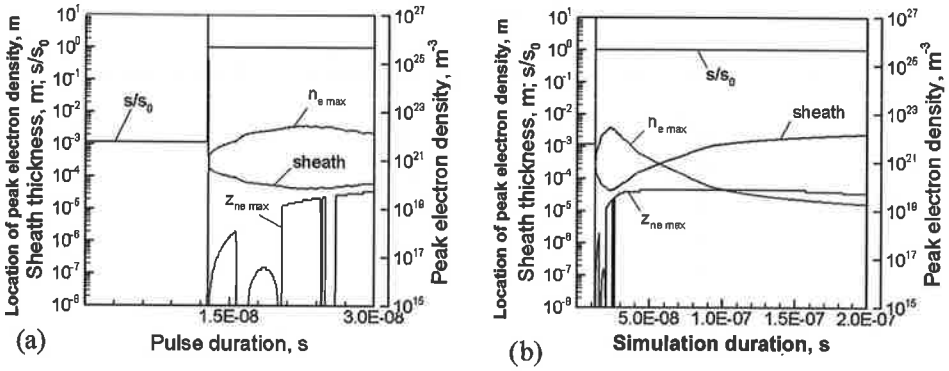

Fig. 6. Transient electrostatic sheath using 9-kV bias voltage in thermally ionized plasma generated by ablation of Al with laser fluence of 4 J/cm^2 in N_2 background maintained at 1-atm: (a) during pulse and (b) beyond pulse.

The optimum wavelengths specified above are all based on single-pulse ablation. If there are multiple pulses, the plasma density in the plume increases and the rate of increase depends on the time lag between successive pulses. If the time lag is large, then the plasma created by a previous pulse will expand out, giving way to the plasma generated by the new pulse. On the other hand, if the time lag is shorter than the expansion time, the plasma created by a new pulse will add to that created by the previous pulse and the overall density increases. Figure 4 shows that wavelength converges to a single optimum value at higher plasma densities. So, the optimum wavelength calculated for a single pulse may be extended to multiple pulses with the loss of some accuracy.

3.2. Electrostatic sheath

At a particular time instant, the peak density of electrons and its location are found in the plume domain. Using these parameters as inputs, for a given value of U, sheath thickness is obtained at all time instances. Sheath characteristics for Al and Ti plasma in N_2 background maintained at 1-atm pressure are discussed first, and then the effect of background pressure on sheath requirements in Al plasma are discussed.

The transient sheath characteristics of Al plasma generated with a laser fluence of 4 J/cm^2 using bias voltage of 9 kV are shown in Fig. 6. The subplots show the instantaneous peak density of electrons, location of peak density, ratio s/s_0, and s. Figure 6a shows the simulation carried out during a laser pulse of 30 ns. Plasma starts to develop from 10 ns onward. The density of the electrons increases as the pulse progresses, and it decreases toward the end of the pulse as the energy of the pulse decreases. The location of peak electron density varies from 10^{-8} to 5×10^{-4} m. The ratio s/s_0 varies from 10^{-3} to 1, and a sudden jump can be seen at the location where electron density builds up. It is shown that within this time scale and at lower values of n_e, transient sheath calculations are required, whereas at higher n_e, Child–Langmuir sheath calculations are sufficient. During the first 10 ns, s is very large as n_e is small, and as time progresses, n_e increases and s decreases. Figure 6a shows clearly that s is greater than the location of peak density within the pulse duration of 30 ns. After the laser pulse is stopped, the plasma formed at the surface continues to expand to the background pressure, whereas the peak density of

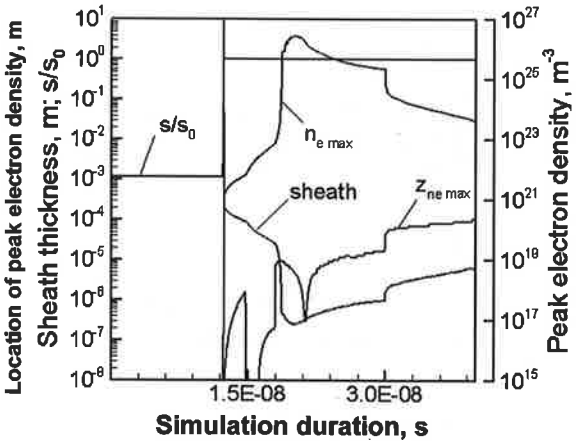

Fig. 7. Transient electrostatic sheath using 10-kV bias voltage in thermally ionized plasma generated by ablation of Al with laser fluence of 4.5 J/cm^2 in N_2 background maintained at 1 atm.

electrons decreases continuously due to the recombination of electrons and ions. The sheath thickness increases as the peak density of electrons decreases, and Fig. 6a shows that it is always larger than the location of peak density of the electrons. In summary, Fig. 6 shows that electromagnetic waves can be transmitted through Al plasma generated with 4-J/cm^2 fluence and 1-atm background pressure.

The sheath characteristics with laser fluence of 4.5 J/cm^2 and $U = 10$ kV are shown in Fig. 7. At this laser fluence, n_e is very high ($\approx 10^{26}$ m^{-3}) and hence the sheath thickness is small and smaller than the peak density location. Although the sheath thickness can be increased by increasing U, due to the limitations involved in onboard voltage sources, the maximum allowable value for U is 10 kV.

A similar analysis is carried out for ablation of Ti to find the fluence limit up to which the electrostatic sheath can be applied. The sheath characteristics are shown in Fig. 8. It can be seen from Fig. 8a that the sheath thickness is greater than the maximum n_e location for a fluence of 1.3 J/cm^2 and $U = 1$ kV. Figures 8b and 8c show that the sheath thickness for a slightly higher fluence of 2 J/cm^2 and with $U = 1$ and 10 kV is smaller than the peak n_e location. Hence the electrostatic approach can be used for Ti plasma during laser ablation with fluences up to 1.3 J/cm^2 only.

The peak electron density history of Al plasma generated using a laser fluence of 4 J/cm^2 in N_2 background with pressure varying from 10^5 to 10^2 Pa is shown in Fig. 9. The electron density increases with the decrease in pressure up to 10^4 Pa and then decreases with the further decrease in pressure up to 10^2 Pa. When the background pressure is decreased, the shock strength increases, which results in higher temperatures, whereas the vapor density decreases due to increased plume length. Although there exists a high density of N_2 at the shock front, the ionization rates are negligibly small due to its high ionization potential. So, there exists a certain value of background pressure for which electron density is maximum. For the present regime, this pressure is found to be around 10^4 Pa.

The sheath thickness and location of the peak density of electrons are shown in Fig. 10 for four different background pressures with a bias voltage of 9 kV. For the case of 7.5×10^4 Pa background pressure (Fig. 10a), the sheath thickness is greater than the location of the

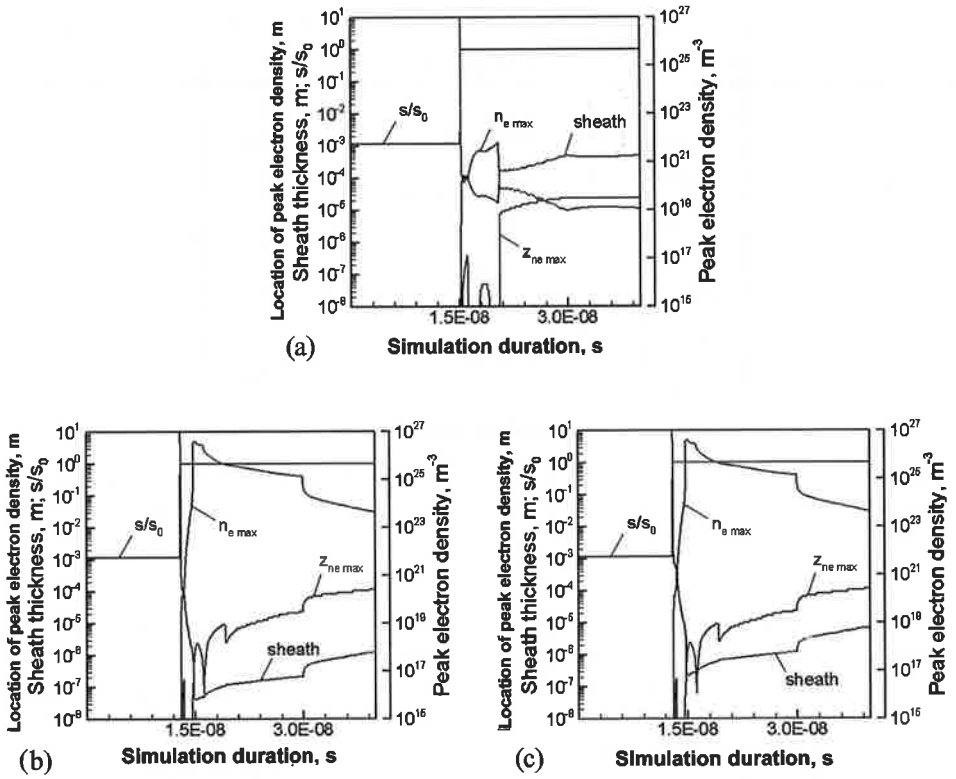

Fig. 8. Transient electrostatic sheath in thermally ionized plasma generated through laser ablation of Ti in N_2 background maintained at 1 atm: (a) laser fluence 1.3 J/cm^2 and bias voltage 1 kV, (b) laser fluence 2 J/cm^2 and bias voltage 1 kV, and (c) laser fluence 2 J/cm^2 and bias voltage 10 kV.

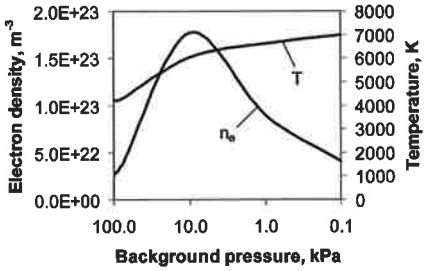

Fig. 9. Effect of background pressure on plasma electron density and temperature.

peak density of electrons at all time instances. The sheath thickness is smaller than the peak electron density location for the remaining three background pressures, 10^4, 10^3, and 10^2 Pa, shown in Figs. 10b–10d, respectively. Because electron density is highest for a background pressure of 10^4 Pa, the sheath thickness is smallest. Although electron densities and sheath thickness for the cases of 7.5×10^4 and 10^2 Pa background pressure are of the same order, the location of the peak electron density is farther for the latter case

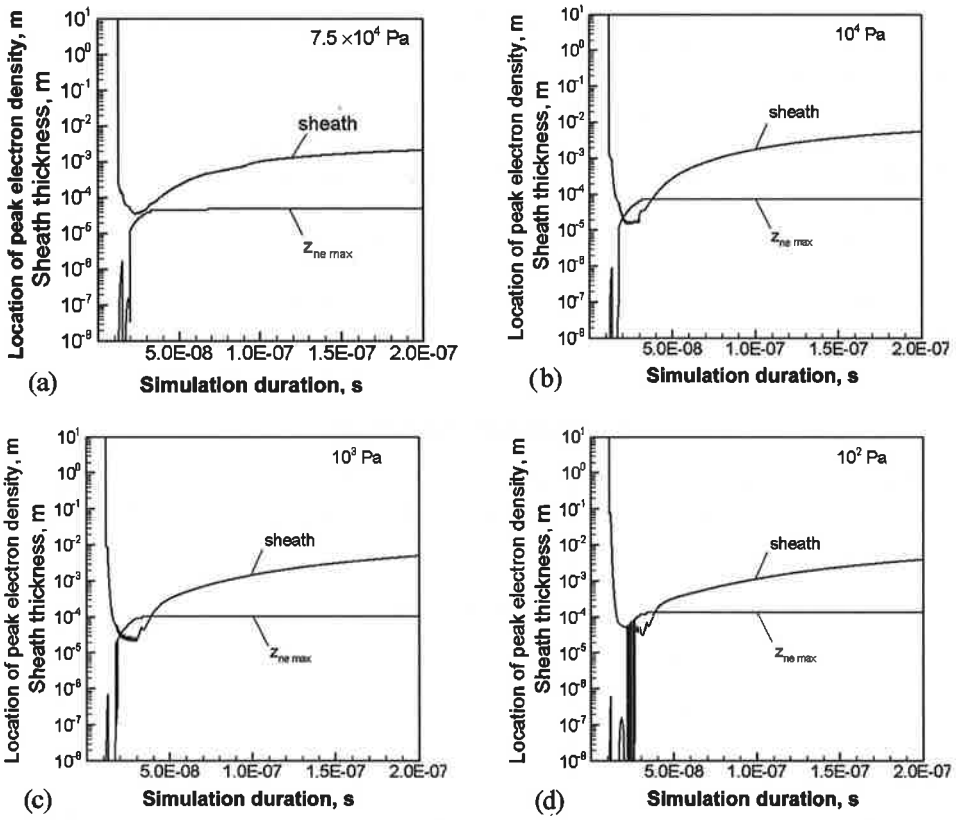

Fig. 10. Effect of background pressure on location of peak density of electrons and electrostatic sheath during laser ablation of Al alloy with fluence of 4 J/cm^2. Bias voltage is 9 kV and background gas is N_2. Calculations are performed with four different background pressures: (a) 7.5×10^4, (b) 10^4, (c) 10^3, and (d) 10^2 Pa.

due to the longer plume. So, the sheath thickness is smaller than the location of the peak electron density in the case of 10^2-Pa background pressure. From this analysis it can be derived that the bias voltage requirement increases with the increase in altitude as pressure decreases.

4. Conclusions

Numerical analysis is carried out to obtain the optimum wavelength for laser-based DEWs to maximize the depth of ablation of three different materials, Al, Cu, and Ti. The analysis shows that the depth of ablation is high for the wavelength for which surface reflectivity lies in medium-range values. The optimum wavelength changes from material to material. The optimum wavelength for Al is 850 nm. Two optimum wavelengths are noticed for Cu and Ti in low (10–50 J/cm^2)- and high (50–100 J/cm^2)-fluence ranges due to the variation in the material absorption coefficient. So, the optimum wavelengths for Cu are 360 and 460 nm in low- and high-fluence ranges. Similar values for Ti are 760 and

532 nm, respectively. The maximum depth of ablation of the three materials is found to be 1.1, 0.8, and 1.4 μm, respectively. Although Ti has superior heat sink properties compared to Al and Cu, it undergoes the highest depth of evaporation.

The electrostatic sheath approach is found to be useful for the mitigation of communication attenuation during testing of DEWs with relatively low laser fluences. Sheath characteristics change significantly with the change of fluence and target material. The transient sheath analysis carried out for Al and Ti targets shows that the electrostatic sheath can be used for ablation of Al targets with fluences up to 4 J/cm^2 and for Ti targets with 1.3 J/cm^2 with a maximum bias voltage of 10 kV in 1-atm background pressure. It is found that the bias voltage requirement increases with the decrease in background pressure.

5. Acknowledgment

The authors gratefully acknowledge the support of the Air Force Office of Scientific Research, Grant No. FA9550-08-1-0343. Dr. John Schmisseur is the technical manager.

References

[1]Amoruso, S., R. Bruzzese, N. Spinelli, and R. Velotta, J. Phys., At. Mol. Opt. Phys. **32**(14), R131 (1999).

[2]Army Test and Evaluation Command, Aberdeen Proving Ground, MD, "Directed Energy Weapons Testing Raises Issues," ADA323342, March 20, 1997.

[3]Barthélemy, O., J. Margot, M. Chaker, M. Sabsabi, F. Vidal, and T.W. Johnston, Spectrochim. Acta, Part B **60**(7–8), 905 (2005).

[4]Beilis, I.I., IEEE Trans. Plasma Sci. **13**(5), 288 (1985).

[5]Bogaerts, A., and Z. Chen, Spectrochim. Acta, Part B **60**(9–10), 1280 (2005).

[6]Child, C.D., Phys. Rev. (Ser. I) **32**, 492 (1911).

[7]Dou, K., E.T. Knobbe, R.L. Parkhill, and Y. Wang, IEEE J. Selected Topics Quantum Electronics **6**(4), 689 (2000).

[8]Hudson, R.D., Jr., *Infrared Systems Engineering*, p. 115, Wiley, New York (1969).

[9]Keidar, M., I.D. Boyd, and I.I. Beilis, J. Phys. D **34**, 1675 (2001).

[10]Keidar, M., and I.G. Brown, J. Vac. Sci. Technol. B **17**(6), 2648 (1999).

[11]Keidar, M., J. Fan, and I.D. Boyd, J. App. Phys. **89**(6), 3095 (2001).

[12]Keidar, M., M. Kim, and I.D. Boyd, J. Spacecraft Rockets **45**(3), 445 (2008).

[13]Keidar, M., M. Kundrapu, M. Kim, I.D. Boyd, C.H. Jones, and B. Mork, "Approaches to Mitigate Disruption of Telemetry during Directed Energy Testing," Proceedings of 44th Annual International Telemetering Conference, San Diego, CA, 27–30 October 2008.

[14]Kim, M., M. Keidar, and I.D. Boyd, IEEE Trans. Plasma Sci. **36**(4), 1198 (2008).

[15]Knight, C.J., AIAA J. **17**(5), 519 (1979).

[16]Krishnan, S., and P.C. Nordine, Phys. Rev. B **48**(6), II (1993).

[17]Kundrapu, M., and M. Keidar, J. App. Phys. **105**, 083302 (2009).

[18]Lide, D.R., and H.P.R. Frederikse, *Handbook of Chemistry and Physics*, 76th ed., CRC Press, Boca Raton, FL (1995–1996).

[19]Rybak, J.P., and R.J. Churchill, IEEE Trans. Aerospace Electronic Syst. AES-**7**(5), 879 (1971).

[20]Semak, V.V., and T.F. Miller, J. Directed Energy **2**(1), 5 (2006).

[21]Semerok, A., B. Sallé, J.F. Wagner, and G. Petite, Laser Particle Beams **20**(1), 67 (2002).

[22]Sprangle, P., J.R. Penano, A. Ting, B. Hafizi, and D.F. Gordon, J. Directed Energy **1**(1), **73** (2003).

[23]Weichel, H., *Laser Beam Propagation in the Atmosphere*, Tutorial Text TT03, SPIE, Bellingham, WA (1990).

[24]Weise, T.H.G.G., M. Jung, D. Langhans, and M. Gowin, "Overview of Directed Energy Weapon Developments," 2004 12th Symposium on Electromagnetic Launch Technology, IEEE, Piscataway, NJ (2004).

[25]Zel'dovich, Y.B., and P.Y. Raiser, *Physics of Shock Waves and High-Temperature Hydrodynamics Phenomena*, Dover, New York (2002).

The Authors

Dr. Charles Jones received a B.A. from Bucknell University and a Ph.D. from Washington State University in mathematics. He has more than 23 years of experience in the aerospace industry. He currently works for the Engineering Division at Edwards Air Force Base as an Instrumentation Research Coordinator. He is involved in long-term planning to research and develop new technologies for test and evaluation of aircraft. The requirement for real-time telemetry has led him to sponsor several projects related to communicating through plasmas during plasmasonic flight and directed energy testing. Other interests include juggling and origami.

Dr. Michael Keidar is Associate Professor at the George Washington University. He received the M.Sc. degree with honors from Kharkov Aviation Institute, Ukraine, in 1989 and the Ph.D. degree from Tel Aviv University, Israel, in 1997. He was a Fulbright and Welch Postdoctoral Fellow at Lawrence Berkeley National Laboratory, Berkeley, California; a Research Associate at Cornell University, Ithaca, New York; and a Research Scientist and Adjunct Professor at the University of Michigan, Ann Arbor. His research concerns advanced spacecraft propulsion, plasma-based nanotechnology, plasma medicine, plasma–material interactions, and plasma processing. He has authored more than 120 journal articles. He serves as a Guest Editor of the *IEEE Transaction on Plasma Science*. He is a senior member of IEEE, an Associate Fellow of AIAA, and a member of APS.

Mr. Madhusudhan Kundrapu is a doctoral candidate at the George Washington University, Washington, D.C. He received his master's from the National Institute of Technology Calicut, Calicut, India, in 2004. From 2004 to 2007 he was a scientist at the Indian Space Research Organisation, Trivandrum, India. His areas of research include simulation of plasmas, synthesis of nanostructures, telemetry in hostile environments, and design of thermal protection systems for hypersonic vehicles.